Rotating helical turbulence: three-dimensionalization or self-similarity in the small scales?

2011 J. Phys.: Conf. Ser. 318 042015

(http://iopscience.iop.org/1742-6596/318/4/042015)

Journal of Physics: Conference Series **318** (2011) 042015 doi:10.1088/1742-6596/318/4/042015

Rotating helical turbulence: three-dimensionalization or self-similarity in the small scales?

A. Pouquet[1], J. Baerenzung[2], P.D. Mininni[1,3], D. Rosenberg[1] and S. Thalabard[1,4]

[1]Computational and Information Systems Laboratory, NCAR, Boulder, USA
[2] Interdisciplinary Center for Dynamics of Complex System, Postdam, Germany
[3]Departamento de Física, Facultad de Ciencias Exactas y Naturales, Universidad de Buenos Aires, and IFIBA, CONICET, Ciudad Universitaria, 1428 Buenos Aires, Argentina.
[4] CEA, L'Orme les Merisiers, F–91191 Gif sur Yvette cedex, Saclay, France.

E-mail: pouquet@ucar.edu, baeren@voila.fr, mininni@df.uba.ar, duaner@ucar.edu, simon.thalabard@gmail.com

Abstract. We present numerical evidence on how three-dimensionalization is recovered at small scale in rotating turbulence with helical forcing provided by a Beltrami flow. The relevant ranges (large-scale inverse cascade of energy, anisotropic and isotropic direct cascades of energy and helicity, dissipative) are each moderately resolved. These results stem from large direct numerical simulations on grids of either 1536^3 or 3072^3 points. In the latter case, the scale at which the inertial wave time and the eddy turn-over time are equal is found to be more than one order of magnitude larger than the dissipation scale. We also examine how the presence of such an intermediate scale could affect truncation due to the use of a helical spectral Large Eddy Simulation procedure which can allow for extending the analysis to a wider range of parameters. Finally, the self-similarity of the direct cascade of energy to small scales for rotating flows, observed recently in numerical simulations as well as in several laboratory experiments, will be discussed briefly for its scaling properties and its conformal invariance.

1. Introduction

Rotating turbulence, present in many astrophysical and geophysical flows be it only because of conservation of angular momentum as interstellar molecular clouds contract under their own gravity, has been studied in detail for many years, using a variety of tools: theory (the weak turbulence regime amenable to closure), experiments and observations, numerical simulations and models (see, e.g. for review Cambon, Rubinstein & Godeferd, 2004; Bellet et al., 2006; Bourouiba, 2007). However, the role of velocity-vorticity correlations, or helicity–an invariant in the ideal case (see for review Moffatt & Tsinober, 1992)–is not as well elucidated. Indeed, it is difficult to assess since it involves small-scale derivatives. Its potential importance in atmospheric dynamics was recognized early on (Lilly, 1986); it is measured in hurricanes (Xu & Wu, 2003), and its spectrum in the planetary boundary layer follows a Kolmogorov law (Koprov, 2005). In this context, we give here a rapid overview of some of the recent issues that have emerged when examining such flows at high numerical resolution.

2. Resolving the Zeman scale

The effect of rotation is strong when the Rossby number $Ro = U_0/[L_0\Omega]$ is small, i.e. when the time-scale associated with inertial waves is small compared with the nonlinear turn-over time; here, U_0 and L_0 are characteristic velocity and scale, and Ω is the strength of the imposed rotation. At large scale, it is known that the flow undergoes an inverse cascade (see e.g. Smith, Chasnov & Waleffe, 1996) and is anisotropic, organizing in columnar structures, which were shown recently to be highly helical as well (Mininni & Pouquet, 2010b).

However, these two times do not vary in the same fashion with scale, and thus, there exists a scale, which we call the Zeman scale (Zeman, 1994) $\ell_\Omega = 2\pi/k_\Omega$, at which $Ro \sim 1$, that is nonlinearities and rotation become comparable. Isotropization and a traditional Kolmogorov scaling may well occur at smaller scales, whereas the large scales are presumably dominated by nonlinear dynamics modulated by waves and in which the role of helicity has been shown recently to be essential (see Mininni & Pouquet, 2010a,b). Note that we are not talking here of isotropization occurring in the dissipative range, as has been found in some cases, but in the inertial range; in other words, the condition $\tau_\Omega < \tau_{diss}$ must be fulfilled, equivalent to $Ro < Re$, a condition that is met in most astro-geophysical flows. It is easy to find phenomenologically that, with $\epsilon = DE/DT$ the energy injection rate, $\ell_\Omega = [\Omega^3/\epsilon]^{1/2}$ (Dubrulle & Valdetarro, 1992; Zeman, 1994), including in the helical case (Mininni, Rosenberg & Pouquet, 2011). We present in this paper evidence for isotropization in a small scale inertial range, and we study as well statistical properties of the self-similar regime induced by the cascade of helicity (see also Mininni, Rosenberg & Pouquet, 2011).

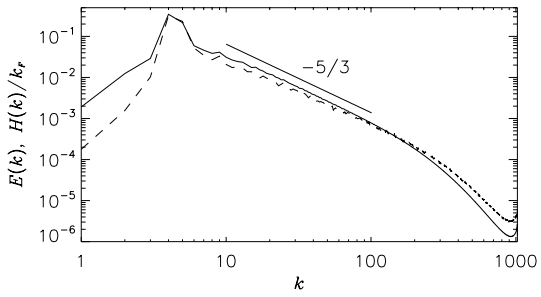

Figure 1. Spectra of energy (solid line) and helicity normalized by the forcing wavenumber $k_F = 4$ (dashed line), for run R2 with weak rotation ($\Omega = 0.06$). The straight line follows a Kolmogorov $k^{-5/3}$ law, which is observed for both spectra in this weak Ω case.

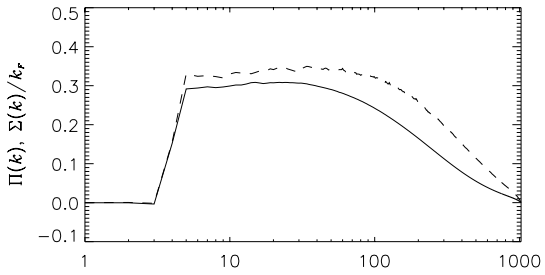

Figure 2. Spectral variation of the fluxes of energy (solid line) and normalized helicity (dashed line) at the same time as in Fig. 1, i.e. at the end of this preliminary phase of the computation. Observe the absence of flux at scales larger than the forcing.

2.1. Preliminaries: the case of weak rotation

We integrate numerically the Navier-Stokes equations in the rotating frame of reference, with the Coriolis force acting on the flow of velocity $\mathbf{u}$, assumed incompressible, $\nabla \cdot \mathbf{u} = 0$:

$$\frac{\partial \mathbf{u}}{\partial t} + \boldsymbol{\omega} \times \mathbf{u} + 2\boldsymbol{\Omega} \times \mathbf{u} = -\nabla \mathcal{P} + \nu \nabla^2 \mathbf{u} + \mathbf{F} \ , \tag{1}$$

where $\mathcal{P}$ is the total pressure modified by the centrifugal term, $\omega = \nabla \times \mathbf{u}$ is the vorticity, and the rotation Ω is imposed in the vertical direction; $\mathbf{F}$ is a fully helical (and still isotropic

although not invariant under plane symmetry) Beltrami forcing centered around $k \sim k_F$, using the so-called ABC flow; finally, the Reynolds number is $Re = U_0 L_0/\nu$ with ν the kinematic viscosity. Note that no polarization anisotropy (see eq. (6) in Cambon & Jacquin, 1989) is introduced by this forcing since it is maximally helical: energy and helicity Fourier spectra $E(k)$ and $H(k)$ for the forcing have $H(k) = kE(k)$ (see also equation (2)).

Two direct numerical simulations (DNS) are discussed in this paper, on grids of respectively 1536^3 points (R1) and 3072^3 points (R2), with $k_{F,R1} = 7$ (Mininni & Pouquet, 2010a,b), and $k_{F,R2} = 4$ (Mininni, Rosenberg & Pouquet, 2011); their respective Reynolds and Rossby numbers are $Re^{R1} \approx 5.1 \times 10^3$, $Re^{R2} \approx 2.7 \times 10^4$, $Ro^{R1} \approx 0.06$, $Ro^{R2} \approx 0.07$. Note that Large Eddy Simulation (LES) runs performed for run R2 are also briefly analyzed in §3. For both DNS runs, we first started with negligible rotation ($Ro \approx 8.5$) and let the flows establish a statistically steady state: a Kolmogorov spectrum obtains for both the energy and the helicity normalized by the forcing wavenumber (see Fig. 1 for R2), and the fluxes are constant at small scales and equal to zero at scales larger than the forcing (see Fig. 2); note the slight domination of the helicity flux, likely a trace of the weak rotation. We now introduce rotation at a time labelled $t = 0$, and study the further evolution of such flows using a pseudo-spectral code parallelized with a hybrid method (Mininni, Rosenberg, Reddy, & Pouquet, 2011), as discussed next.

2.2. Temporal data in the strong rotation case for $t \geq 0$

We show the total energy and dissipation, $E(t)$ and $Z(t) = 2\nu \int k^2 E(k) dk$, as a function of time, in Fig. 3 and Fig. 4 respectively, for R1 (solid line) and R2 (dashed line). R1 is allowed to evolve for a long time to observe the build-up of the inverse cascade of energy, weaker in R2 due to the proximity of k_F^{R2} with the gravest mode, $k_{min} = 1$. Scales smaller than the forcing scale have stabilized in Run 2 (not shown) but larger scales do display some growth in time. Note that it takes longer in rotating turbulence for dissipation to completely stabilize, compared to standard turbulence, since the energy spectrum is slightly steeper than k^{-2} (Mininni & Pouquet, 2009). The Taylor Reynolds number has saturated for this flow at $t \sim 4$, with $R_\lambda \approx 4500$, whereas by $t = 7$, the integral scale has almost doubled.

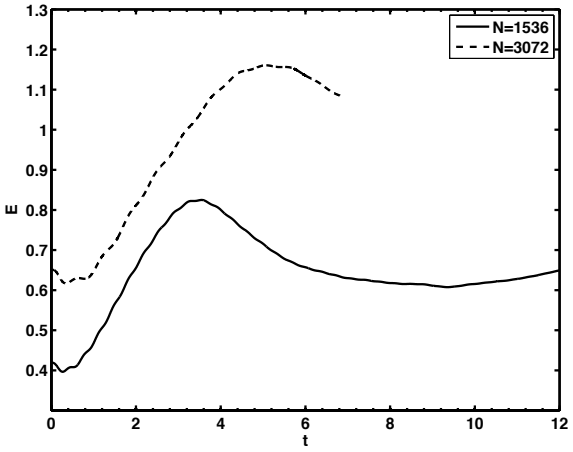

Figure 3. Energy for DNS runs on grids of 1536^3 (R1, solid line) and 3072^3 (R2, dashed line) points, as a function of time. Note the slow growth at the end for R1, indicative of the slow build-up of the inverse cascade.

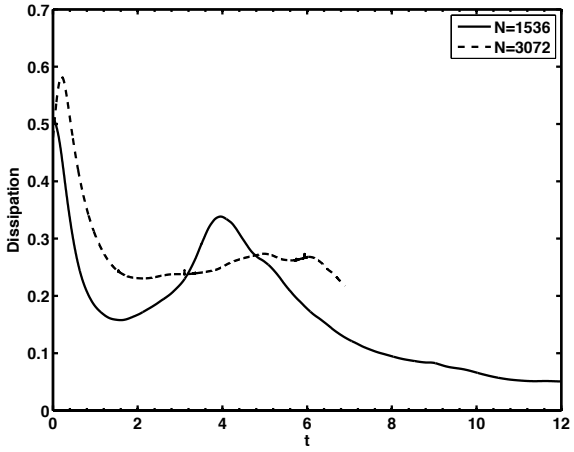

Figure 4. Dissipation as a function of time, for the same DNS runs as in Fig. 3. Note the similar time scales for both flows which have similar Rossby numbers, as the dynamics adjust to the stronger imposed rotation.

2.3. Spectra and fluxes in the presence of strong rotation

The overall global temporal similarities between runs R1 and R2 does lead, however, to different dynamics when examining the repartition of energy and helicity among scales with the help of their isotropic Fourier spectra, $E(k)$ and $H(k)$, with $\int E(k)dk = E = \frac{1}{2} < |u^2| >$, $\int H(k)dk = H =< \mathbf{u} \cdot \omega >$. Spectra are built-up from their axi-symmetric counterparts defined from the two-point one-time velocity covariance $U(\mathbf{k})$, with ϕ the longitude with respect to the x axis:

$$e(|\mathbf{k}_\perp|, k_\parallel) = \Sigma_{k_\perp \leq |\mathbf{k}\times\hat{\mathbf{z}}| \leq k_\perp+1} \; U(\mathbf{k}) = \int U(\mathbf{k})|\mathbf{k}| \sin\theta d\phi \; = e(|\mathbf{k}|, \theta) \; , \tag{2}$$

and with θ the co-latitude in Fourier space with respect to the vertical axis with unit vector $\hat{\mathbf{z}}$. Here, $k_\perp$ and $k_\parallel$ refer to the direction of rotation, i.e. the vertical axis; $\theta = 0$ corresponds to $e(|k_\perp| = 0, k_\parallel)$, and $\theta = \pi/2$ to $e(|k_\perp|, k_\parallel = 0)$, i.e. the so-called slow manifold, since when $k_\parallel = 0$, the waves have zero frequency; similar definitions hold for $h(|k_\perp|, \theta)$. Note that in the definition of contour lines of axisymmetric spectra, a trigonometric factor $1/\sin\theta$ is included in order to allow measuring the density of energy and of helicity, contained in circles of radius $k \sin\theta$ (note that for a fully isotropic flow, this density is independent of θ so that circles obtain in that case).

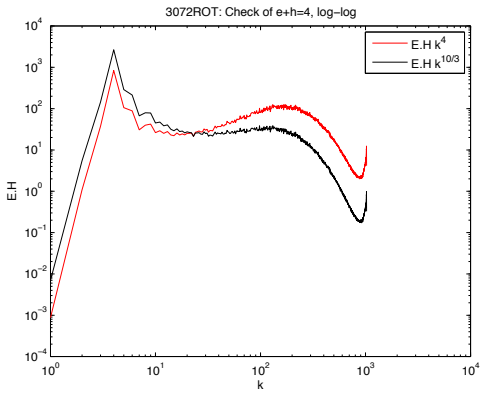

Figure 5. Spectral product $E(k)H(k)$, compensated by either k^4 (red line) or $k^{10/3}$ (black), corresponding respectively to the new helically-dominated wave-modulated regime at large scale (Mininni & Pouquet, 2010b) or to a dual Kolmogorov law at smaller scale, each moderately resolved. Note the quasi-absence of bottleneck.

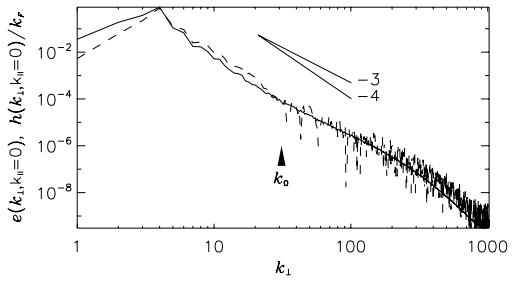

Figure 6. Anisotropic spectra of energy (solid line) and helicity (dashed line) in the slow manifold ($k_\parallel = 0$), the latter normalized by k_F, as a function of $k_\perp$, where directions refer to the vertical rotation axis. The arrow gives the Zeman wavenumber k_Ω. Note the breakdown of the helicity spectrum beyond k_Ω.

It is known that nonlinear transfer to small scales is slowed-down in the presence of waves. This can be modeled by an argument first put forward in Dubrulle & Valdetarro (1992) (see also Zhou, 1995) for rotating flows; the resulting spectrum is $E(k) \sim [\epsilon\Omega]^{3/2}k^{-2}$. In the presence of helicity, it was found that the small-scale cascade is dominated by helicity and one should take into account instead its own rate of dissipation, namely $\tilde{\epsilon} \equiv dH/dt$; dimensionally, this leads to $e + h = 4$ with e and h the inertial indices for energy and helicity, and with $e = h = 2$ in the non-helical case. This new law, with some evidence that $e \neq h$, was presented in Mininni & Pouquet (2010a). We show in Fig. 5 that it seems again to be valid at large scale, on a small range of scales, but that at smaller scale a Kolmogorov law seems to be recovered, with a transition around $k \approx 30$; an evaluation of the Zeman scale yields $k_\Omega = \left(\Omega^3/\epsilon\right)^{1/2} \sim 30$,

in rather close agreement with the numerical data. Note that the phenomenological argument gives a prediction for the spectral product $E(k)H(k) \sim k^{-4}$, but not for the individual spectra themselves. In the case of maximal helicity throughout the range ($H(k) = kE(k)$), we would have $e = 5/2,\ h = 3/2$, a state that is not reached in this computation and which is known to be unstable in the non-rotating case (Podvigina & Pouquet, 1994).

Furthermore, when we examine the anisotropic spectra of energy and helicity (see Fig. 6) in the case of $k_\parallel = 0$, we see that not only is there a break in the slope of these spectra around k_Ω, but also that for $k > k_\Omega$, the helicity spectrum looses its coherence of sign; we can infer from this that the small scales are helical, but with structures in which velocity and vorticity are either parallel or anti-parallel, a known feature in the non-rotating case.

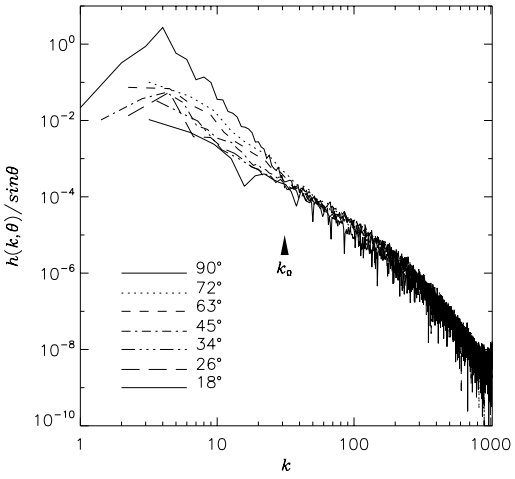

Figure 7. Helicity spectrum for several co-latitudes θ (see for definitions Mininni, Rosenberg & Pouquet, 2011). For $k < k_\Omega$ (shown with an arrow), anisotropy prevails.

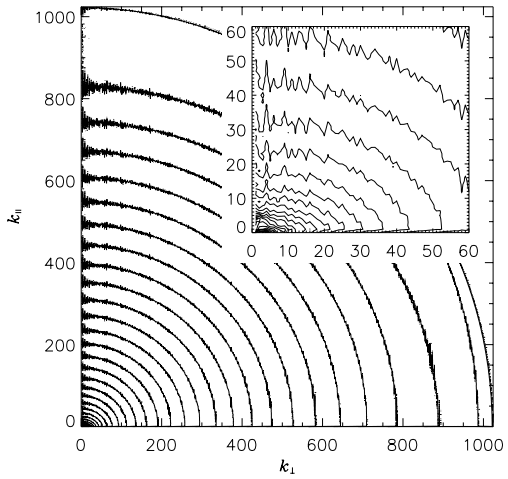

Figure 8. Angular energy spectrum, with a blow-up for the large scales in the inset, with anisotropy showing up in the form of elliptic contour lines.

Angular spectra are shown in Fig. 7 for the helicity, the corresponding spectra for energy being discussed in Mininni, Rosenberg & Pouquet (2011). Again, a marked transition is seen in the vicinity of the Zeman wavenumber, indicated by an arrow in the figure: at large scales, there is a substantial variation of energy distribution with co-latitude, whereas at sufficiently small scales, isotropy does seem to recover way before the dissipation range that occurs close to the cut-off $k_{max} = 1024$. Finally, in Fig. 8 is given a contour plot of the angular energy spectrum in terms of $|k_\perp|$ and $k_\parallel$, with in the inset a large-scale zoom displaying the anisotropic (ellipsoidal) contour lines at the largest scales.

2.4. Structures

One of the striking findings of our preceding study of helical rotating turbulence is the appearance of fully helical large-scale columnar structures, which we coined Beltrami Core Vortices, or BCV. What happens when isotropization is recovered at small scale? We see in Fig. 9 a perspective volume rendering (PVR) of the vertical component of the velocity; red-green are for negative values, and blue-purple for positive values of similar magnitudes, corresponding for u_z to updrafts. The figures are performed using the VAPOR freeware (Clyne et al., 2005) allowing for loss-less wavelet compression of the data and different available resolutions for rendering.

The helicity at the same time and with the same angle of view is given in Fig. 10, and a zoom using a higher graphical resolution is displayed in Fig. 11.

One feature not present in our preceding simulation R1, is the fact that, at times, the complex small-scale downdrafts seems to wrap around the more organized vertical updraft. The origin of such a behavior is unknown at the present time. The evidence for columnar structures is less clear in the helicity PVR given in Fig. 10. The helicity is dominated by small scales which are isotropic on average but the large-scale columnar organization is still clearly detectable.

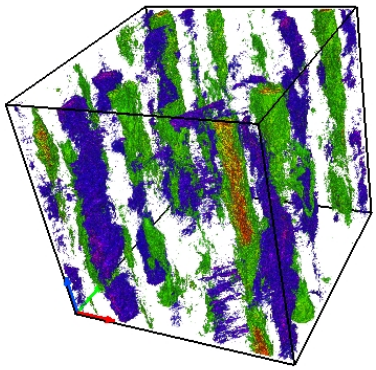

Figure 9. Vertical velocity u_z above a given threshold using Perspective Volume Rendering (PVR) at $t = 6.7$ for R2 (3072^3 resolution), with red-green for negative, and blue-purple for positive (updraft). Observe the columns due to rotation and the wrapping of some vortices around them.

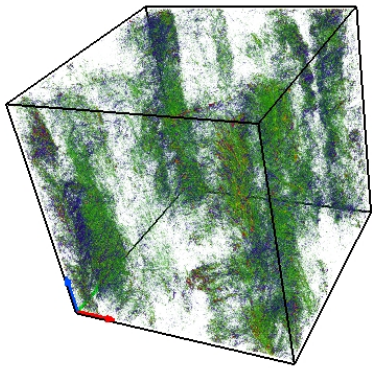

Figure 10. Helicity PVR at the same time as Fig. 9. The columns seen in u_z are still discernible, but the isotropization of the small scales observed in the angular spectra of Figs. 7 and 8 is responsible for the overall fuzzyness of the columns, compared to run R1 for which $k_\Omega \sim k_{diss}$.

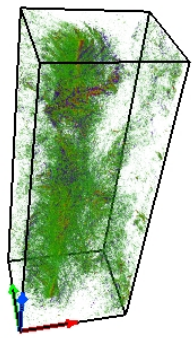

Figure 11. PVR zoom, with enhanced graphical resolution using VAPOR (Clyne et al., 2005); note the wrapping around of vortex filaments (at the top, mostly blue slightly slanted vortex bunch), also present in the u_z zoom (not shown).

3. Modeling of rotating turbulence when the Zeman scale is resolved

It would be of interest to study such complex rotating flows in greater detail, in particular resolving better each of the relevant ranges (large-scale inverse cascade, barely existent for run R2, the direct anisotropic and the direct isotropic energy and helicity cascades and the dissipative range), but the cost may be prohibitive. One way around such a difficulty is to use Large-Eddy Simulations (LES) which have been developed over the years for turbulent flows (see e.g. the review in Cambon & Scott, 1999), including in the rotating helical case. But a question arises as to wether there is a need to resolve sufficiently in detail the Zeman scale in the LES run in order to model the turbulent flow accurately. To address this, we conducted a series of LES runs using the helical spectral model developed in Baerenzung et al. (2011), at various resolutions,

128^3, 256^3 and 512^3 grid points, and respective cut-off wavenumbers 64, 128 and 256 with the intention of comparing them to run R2. Recall that, in this model, the energy spectrum of the resolved part is fitted to compute the relevant transport coefficients, namely the eddy viscosity and eddy noise, with their respective symmetric (energetic) and helical components. The fit to the resolved scales occurs over a range from $\frac{3}{4}k_{max}$ to k_{max}. Thus, in all cases, the fit range lies beyond the Zeman scale of run R2, and the fit sees nominally only the isotropic range, though in the first 128^3 case, these scales are quite close. While it is of interest ideally to evaluate all three cases where the fit occurs (1) entirely within the anisotropic range, (2) across the transition, and (3) entirely within the isotropic range, it is somewhat difficult and expensive to produce a DNS that will facilitate such a detailed comparison.

We show now the preliminary results of this study. In Fig. 12, we give the temporal evolution for the three LES runs and for the DNS run R2 (solid line); the LES runs at all resolutions give similar (although not identical) results, with an error at peak of less than 3%. Differences are discernible, though, when examining the spectra displayed in Fig. 13 for the 512^3 resolution, and in the inset for the 128^3 resolution run; the green and red arrows indicate respectively the Zeman scale for the LES and the DNS. Note that all spectral and flux data is averaged in the temporal window $t \in [5.5, 6.5]$. One can see that while the energy does not differ by much, the lower-resolution LES gives neither a good Kolmogrov dual isotropic range ($E(k) \sim k^{-5/3}$, $H(k) \sim k^{-5/3}$), nor a good value for the Zeman scale. The value computed for k_Ω in the 512^3 LES is nearly identical to that from run R2. Finally, Fig. 14 gives the fluxes of energy (in black) and helicity (in red), the latter normalized by the forcing wavenumber $k_F = 4$; the solid line is for the DNS R2 run and the dashed line for the LES run on a grid of 512^3 points, i.e. 6^3 times smaller. Note that the flux is cubic and therefore, the errors are a bit amplified compared to the energy but remain small; this is the probable cause of the larger discrepancy in the values of the fluxes as compared with the energy, although the flux ratio in the LES, which determines in what regime we are, is in rather good agreement with the DNS. We note to conclude this section that such a tool may prove useful in exploring further rotating turbulence, in particular having better resolved inverse and anisotropic direct cascades.

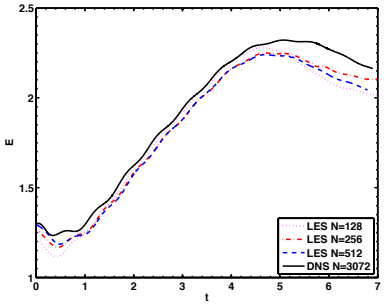

Figure 12. Temporal evolution of energy for the DNS run R2 on 3072^3 grid points (solid line), and for LES runs at resolutions from 128^3 to 512^3 points (see inset, and see also Fig. 3 for the DNS run R1).

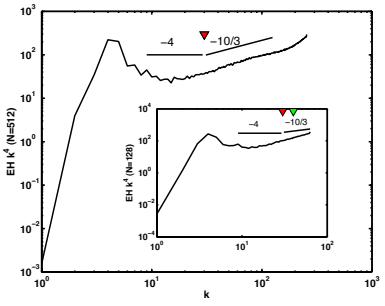

Figure 13. $k^4E(k)H(k)$ time-averaged for $t \in [5.5, 6.5]$ for the 512^3 grid LES run (inset: 128^3-LES); green and red arrows are respectively for k_Ω computed for the LES and R2 DNS runs.

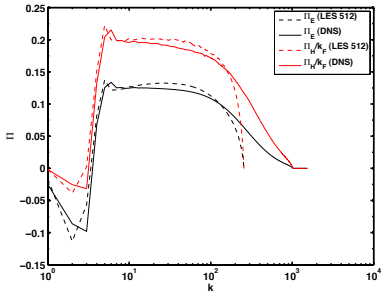

Figure 14. Time-averaged fluxes of energy (black) and helicity (red) for the DNS run R2 (solid) and the LES run on a grid of 512^3 points (dash line); see Fig. 2 for the fluxes in the weakly-rotating DNS .

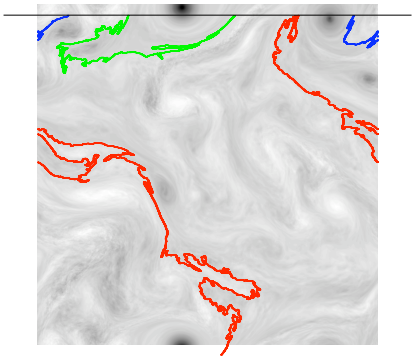

Figure 15. Three different paths (shown in color) of zero-field lines of the vertical component of the vorticity averaged in the vertical, $\langle\omega_z\rangle_z$, all started from the black horizontal line at the top. These paths are super-imposed on the grey-scale display of $\langle\omega_z\rangle_z$ for Run R1 on a grid of 1536^3 points (Thalabard et al., 2011), and are analyzed for their Gaussian properties (see Fig. 16).

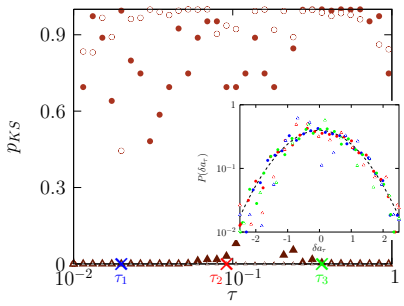

Figure 16. PKS test for Gaussianity for paths similar to those shown in Fig. 15. Inset: probability distribution functions (color dots corresponds to the three path increments $\tau_{1,2,3}$ shown in color), where τs are the pseudo-time associated with the projection of the paths shown in Fig. 15 on the horizontal line using a conformal transformation. A Gaussian is indicated with a dotted line.

4. Conformal invariance

Another striking feature of rotating helical turbulence is the fact that the direct cascade of energy appears to be self-similar, as seen in the numerical study of Run R1 (Mininni & Pouquet, 2010b), and for rotating non-helical flows (Mininni, Alexakis & Pouquet, 2009), as well as in the laboratory (Baroud et al., 2003; Seiwert, Morize & Moisy, 2008; van Bokhoven et al., 2009). Self-similarity is diagnosed by way of a linear variation with order of the scaling exponents ζ_p of structure functions of the velocity, based for example on the longitudinal velocity difference δu_L on a distance r and projected along the distance $\mathbf{r}$, namely $\delta u_L(r) = [\mathbf{u}(\mathbf{x}+\mathbf{r}) - \mathbf{u}(\mathbf{x})] \cdot \mathbf{r}/|r|$. Defining $\langle \delta u(r)^p \rangle \sim r^{\zeta_p}$, self-similarity obtains when $\zeta_p = \gamma p$. One of the unanticipated results of the numerical and experimental investigations was that different γ are obtained for various flows, a feature that can be attributed through a simple phenomenological argument to the presence or not of helicity in the flow, as confirmed in the numerical studies mentioned earlier.

There is evidence in the literature for turbulence in two dimensions that not only it is self-similar (in the inverse cascade), but in fact it is also conformal invariant, a stronger property that involves invariance under change of direction (Bernard et al., 2006). Similarly, one can ask if, in the direct cascade of energy to small scales in three-dimensional rotating turbulence, one can also observe conformal invariance. This can be done by studying the fractal properties of zero-vorticity paths in the flow, once it has been averaged in the direction of rotation. Fig. 15 shows the resulting vertical vorticity averaged in the vertical (direction of rotation) for the run R1 on a grid of 1536^3 points, with $k_F = 7$, $Re \approx 5100$ and $Ro \approx 0.06$; the three different colors correspond to three different paths which are analyzed for their chaotic properties using the so-called Schramm-Löwner evolution (SLE) algorithm (see for review Gruzberg & Kadanoff, 2004; Cardy, 2005). The results show that, indeed, conformal invariance obtains with an associated Brownian diffusion coefficient $\kappa \sim 3.6 \pm 0.1$ (see for more details Thalabard et al., 2011). The Kolmogorov-Smirnov PKS test is performed to verify if the associated process in the complex plane $[x, y]$ is Brownian, checking for Gaussianity, as shown in Fig. 16 for three paths indicated

by different colors (and marked as well on the τ-time axis). This shows that three-dimensional rotating helical turbulence is conformal invariant in the direct cascade, and represents the first known instance of such a process, likely due to the weakened nonlinear interactions with inertial waves. The conformal invariance properties of the inverse cascade are presently under study for another series of runs with forcing at smaller scale.

5. Conclusion

The study of the intermittency properties of the flow of Run R2 is left for future work. One may have to separate the data into the scales larger (resp. smaller) than the Zeman scale to see whether isotropization affects the results of self-similarity, and study the energy as well as the helicity cascade. We expect self-similarity for the large-scale range, but what of the smaller-scale range when the Zeman scale is resolved and isotropy (and thus, presumably intermittency) is recovered? Will there be two ranges for intermittency scaling, as there is clearly for the energy and helicity spectra? Of course, in order to study the combined effect of the inverse cascade of energy (here, barely present), the first anisotropic range and the isotropic range of the direct cascades of energy and helicity, and finally the dissipation range, means that none of these ranges will be well resolved and that further studies will be necessary, either with larger simulations or with the help of models of turbulence, as considered here, or using a divide and conquer approach.

Acknowledgments

Computer time was provided by NSF under TeraGrid Grant No. TG-PHY100029. NCAR is sponsored by the National Science Foundation. We acknowledge support from NSF-CMG Grant No. 1025188, and PDM acknowledges support from PICT Grant No. 2007-02211, UBACYT Grant No. 20020090200692, PIP Grant No. 11220090100825, and from the Carrera del Investigador Científico of CONICET.

References

Baerenzung, J., Mininni, P.D., Pouquet, A. & Rosenberg, D. 2011 Spectral Modeling of Turbulent Flows and the Role of Helicity in the presence of rotation. Online, April issue. *J. Atmos. Sci.* .

Baroud, C. N., Plapp, B. B., Swinney, H. L & She, Z.-S. 2003 Scaling in three-dimensional and quasi-two-dimensional rotating turbulent flows. *Phys. Fluids*, **15**, 2091–2104.

Bellet, F., Godeferd, F.S., Scott, F.S. & Cambon, C. 2006 Wave turbulence in rapidly rotating flows. *J. Fluid Mech.*, **562**, 83–121.

Bernard, D., Boffetta G., Celani A. & Falkovich, G. 2006 Conformal invariance in two-dimensional turbulence. *Nature Phys.* **2**, 124–128.

van Bokhoven, L.J., Clercx, H.J.H., van Heijst, G.J.F., & Trieling, R.R. 2009 Experiments on rapidly rotating turbulent flows. *Phys. Fluids* **21**, 096601.

Bourouiba, L., & Bartello, P. 2007 The intermediate Rossby number range and two-dimensional-three-dimensional transfers in rotating decaying homogeneous turbulence. *J. Fluid Mech.* **587**, 139–161.

Cambon, C., & Jacquin, L. 1989 Spectral approach to non-isotropic turbulence subjected to rotation. *J. Fluid Mech.* **202**, 295–317.

Cambon, C., & Scott, J.F. 1999 Linear and nonlinear models of anisotropic turbulence. *Ann. Rev. Fluid Mech.* **31**, 1-53.

Cambon, C., Rubinstein, R. & Godeferd, F.S. 2004 Advances in wave turbulence: rapidly rotating flows. *New J. Phys.* **6**, 73, 29 pages.

Cardy, J.L. 2005 SLE for theoretical physicists. *Annals Phys.* **318**, 81–118.

Clyne, J., Mininni, P.D., Norton, A. & Rast, M. 2005 Interactive desktop analysis of high resolution simulations: application to turbulent plume dynamics and current sheet formation. *New J. Phys.* **9**, 14 pages.

Dubrulle, B., & Valdetarro, L. 1992 Advances in wave turbulence: rapidly rotating flows Advances in wave turbulence: rapidly rotating flows. *Astronom. Astrophys.* **263**, 387–400.

Gruzberg, I.A. & Kadanoff, L.P. 2004 The Loëwner equation: maps and shapes. *J. Stat. Phys.* **114**, 1183–1198.

Koprov, B., Koprov, V., Ponomarev, V., & Chkhetiani, O. 2005 Experimental Studies of Turbulent Helicity and Its Spectrum in the Atmospheric Boundary Layer. *Doklady Physics* **50**, 419–422. Translated from *Doklady Akademii Nauk* **403**, 627–630 (2005).

Lilly, D. 1986 The Structure, Energetics and Propagation of Rotating Convective Storms. Part II: Helicity and Storm Stabilization. *J. Atmos. Sci.* **43**, 126–140.

Mininni, P.D., Alexakis, A. & Pouquet, A. 2009 Scale interactions and scaling laws in rotating flows at moderate Rossby numbers and large Reynolds numbers. *Phys. Fluids* **21**, 015108.

Mininni, P.D. & Pouquet, A. 2009 Helicity cascades in rotating turbulence. *Phys. Rev. E* **79**, 026304.

Mininni, P.D. & Pouquet, A. 2010a Rotating helical turbulence. Part I. Global evolution and spectral behavior. *Phys. Fluids* **22**, 035105.

Mininni, P.D. & Pouquet, A. 2010b Rotating helical turbulence. Part II. Intermittency, scale invariance and structures. *Phys. Fluids* **22**, 035106.

Mininni, P.D., Rosenberg, D., Reddy, R., & Pouquet, A. 2011 A hybrid MPI-OpenMP scheme for scalable parallel pseudospectral computations for fluid turbulence. *Parallel Computing* **37**, 316–326.

Mininni, P.D., Rosenberg, D. & Pouquet, A. 2011 Two small-scale inertial ranges in rotating helical turbulence and the return to isotropy. submitted to *J. Fluid Mech.*, see also arXiv:1104.5519.

Moffatt, H.k. & Tsinober, A. 1992 Helicity in laminar and turbulent flow. *Ann. Rev. Fluid Mech.* **24**, 281–312.

Podvigina O. & Pouquet A. 1994 On the Nonlinear Stability of the 1:1:1 ABC Flow. *Physica D* **75**, 475–508.

Seiwert, J., Morize, C. & Moisy, F. 2008 On the decrease of intermittency in decaying rotating turbulence. *Phys. Fluids* **20**, 071702.

Smith, L., Chasnov, R. & Waleffe, F. 1996 Crossover from Two- to Three-Dimensional Turbulence. *Phys. Rev. Lett.* **77**, 2467–2470.

Thalabard, S., Rosenberg, D., Pouquet, A. & Mininni, P.D. 2011 Conformal invariance in three-dimensional rotating turbulence. *Phys. Rev. Lett.* **1**06, 204503.

Xu, Y. & Wu, R. 2003 The conservation of helicity in Hurricane Andrew (1992) and the formation of the spiral rainband. *Adv. Atmosph. Sci.* **20**, 940–950.

Zeman, O. 1994 A note on the spectra and decay of rotating homogeneous turbulence. *Phys. Fluids* **6**, 3221–3223.

Zhou, Y. 1995 A Phenomenological Treatment of Rotating Turbulence. *Phys. Fluids* **7**, 2092–2094.